Electrochemical investigation of pre-deformation in AISI 321 stainless steels

LV Jin-long, HAN Yun-tao, and LUO Hong-yun

Department of Materials Science and Engineering, Beijing University of Aeronautics and Astronautics
xueyuan Road 37, Beijing 100191 China (ljlhit@126.com, hanyuntao1985@163.com, luo7128@163.com)

Abstract: This project studied the effect of tensile deformation on the corrosion behavior of an austenitic AISI 321 stainless steel in a 5% NaCl solution, at room temperature. Pre-deformed tensile samples ranging from 6% to 30% were tested. Microstructural changes were analyzed by means of XRD, scanning electron microscope (SEM), and transmission election microscopy (TEM). An explanation of the role of the tensile pre-deformation magnitude in influencing the deformation slip band and martensite transformation, based on the results of scanning electron microscopy and XRD investigations, was proposed. The corrosion resistance of uniaxial tensile pre-deformed stainless steel was evaluated using polarization curves and electrochemical impedance spectroscopy. Results indicated that martensite transformation mechanisms included at least two types of nucleation processes. A nonlinear trend of pitting potential, with increasing deformation, was observed. The relationship between pitting corrosion and deformation structures as regards the tensile pre-deformation magnitude was discussed.

Keyword: 321 stainless steels; tensile pre-deformation; pitting corrosion; electrochemical impedance spectroscopy; martensite transformation

1 Introduction

Austenitic stainless steels (ss) with an approximate composition of 18 **wt**. % chromium, 10 **wt**. % nickel, and with additions of molybdenum, titanium or niobium have been widely used in components designed for high temperature applications like nuclear power stations, boilers, superheaters, and chemical reactors[1]. The pre-deformation of austenitic stainless steel with an face-centered cubic (fcc) lattice structure is unavoidable for the fabrication of such components. Temperature, strain rate, and strain[2] are the important parameters that can affect the deformation mechanism from slip to twinning and hence the deformation microstructure of austenitic ss. Among the material properties, the stacking fault energy (SFE) is one of the most important factors in producing changes in the deformation microstructure in austenitic ss. Due to the difference in SFE, austenitic ss produces a variety of deformation microstructures, such as tangled dislocations[3], dislocation pile-ups[4] at grain boundaries, stacking faults, and twins[5]. In addition, austenitic grades can also be sensitive to martensite transformation induced by cold working at room temperature[6,7]. It was demonstrated that the type of deformation and the rate of deformation strongly influence the degree of the α-martensite phase and of the ε-phase, which has hexagonal close-packed (hcp).

Researchers reported an unclear role of pre-deformation on the localized corrosion resistance of stainless steel. However, the corrosion resistance properties for pre-deformed austenitic ss have not been fully comprehended, and the effect of the martensite quantity on the pitting potential has been contradictorily reported as regards the deformation *e.g.*, increases[8], decreases[9], or non-monotonic[10].

The effect of pre-deformation on the pitting potential (V_{pit}) appeared to be more complicated than expected due to the influence of chloride concentration or to the addition of alloying elements. AISI 321 stainless steel has been widely used in the power-generation industry for pressure vessels in gas-cooled nuclear reactors[11] because it exhibits a good corrosion resistance through the inhibited grain boundary sensitization[11,12]. The addition of Ti prevented the formation of chromium rich carbide precipitates at the grain boundaries, which are known to be deleterious to the corrosion resistance of the stainless

Received date: June 13, 2010
(Revised date: July 1, 2011)

steels by the chromium depletion adjacent to the precipitates[12].

Contradictions persist as regards the detailed relationship of pre-deformation and corrosion resistance. However, there are a few studies on the corrosion resistance of deformed 321 stainless steel. The purpose of this work was to determine the effect of the pre-deformation magnitude on the microscopic structure of 321 austenitic stainless steel and to investigate the effect of the amount of deformation on the corrosion resistance properties, such as passive current, break potential, and electrochemical impedance spectroscopy.

2 Experiment

2.1 Test material and tensile test

The chemical composition of the investigated commercial grade AISI 321 austenitic stainless steel plate of a 2 **mm** thickness is shown in Table 1. The Md_{30} temperature of the material at which 50% of the austenite transforms to martensite, at a true strain of 0.30, calculated from the Eq. (1)[13], was found to be 39.65°C. Tensile tests were carried out on the specimens, with a 60 **mm** gauge length, at a strain rate of 0.001 $\mathbf{s^{-1}}$, at room temperature, using a testing system (SANS±100**kN**) in the normal laboratory environment. Plate samples were strained to pre-set engineering strain levels of 6%, 10%, 20% and 30% respectively.

$$M_{d30} = 497 - 13.7Cr\% - 20Ni\% - 8.1Mn\% - 9.2Si\% - 462(C+N)\% - 18.5Mo\% \quad (1)$$

Table 1 Chemical composition (wt. %) of 321 austenitic stainless steel

C	Si	Mn	P	S	Cr	Ni	Ti
0.050	0.840	1.800	0.024	0.024	17.350	9.120	0.540

2.2 Microcosmic observation

Specimens cut from as received and deformed plates were mechanically polished with successive SiC papers of grain size 500, 1000 and 2000. They were subsequently polished with aluminum oxide (Al_2O_3) powder of a 1**μm** diameter. Metallographic and SEM (JSM5800) observation specimens were electrolytically etched in 10 **wt**. % oxalic acid, according to the ASTM G108-94 standard[14]. X-ray diffraction (Rigaku Ultima IV) analysis, using Cu Kα radiation (4**deg**/**min**), CuKα (0.154056 **nm**) radiation at 40 **kV,** and 40 **mA** was used to assess the effect of strain on the phase transformation response. Specimens for transmission electron microscopy (TEM) were cut from the tested samples, mechanically polished, and 3 **mm** discs were punched. Final thinning was performed by twin-jet polishing in a solution of perchloric acid: ethanol 1:9 at 30 **V** and 5°C. The perforated thin foils were examined in TEM (JEM-2100F) at an operating voltage of 200 **kV**. The volume fraction of α-martensite in the surface layer was evaluated using the following formula[15]:

$$V_{\alpha}' = \frac{(1/n)\sum_{j=1}^{n}(I_{\alpha}^{j\prime}/R_{\alpha}^{j})}{(1/n)\sum_{j=1}^{n}(I_{\gamma}^{j}/R_{\gamma}^{j}) + (1/n)\sum_{j=1}^{n}(I_{\alpha}^{j\prime}/R_{\alpha}^{j})} \quad (2)$$

where n, I and R are, respectively, the number of peaks of the phase used in the calculation, the integrated intensity of the reflecting plane, and the material scattering factor. For a sample, only two phases (γ-austenite and α-martensite) were calculated in this paper.

2.3 Electrochemical test

The specimens were sealed in holders with acid resistant epoxy resin in order to expose to the electrolyte a planar area of 1$\mathbf{cm^2}$. Their pretreatment consisted of mechanical polishing with a fine grade emery paper followed by polishing using a soft cloth with alumina as grinding paste, degreasing in acetone, rinsing with distilled water, and drying in air at room temperature.

The electrochemical cell employed in this study was made of glass beaker with the three electrodes (reference, counter and test electrodes) immersed directly into the test solution. A saturated calomel electrode was used as the reference electrode, and all potentials were referred to this scale. A platinum counter electrode was also used. The electrochemical measurements were performed using CHI660B, controlled by a personal computer. The electrolytes were prepared from analytical grade sodium chloride and deionized water. The experiments were carried out at room temperature in a naturally aerated environment. Before potentiostatic film growth, the

specimens were cathodically polarized at -1.1 **V** for 180 **s** to electro-reduce the alloy surface, removing the native oxide film. The potential was swept in the anodic direction starting from -200 **mV** at a rate of 0.0001667 **V/s,** and the pitting potential (E_{pit}) was defined as the potential where the anodic current density exhibited a sharp and sustained increase from the background passive current density. After the anodic polarization tests, the specimens were examined under optical microscope to ensure that no crevice formation occurred at the interface of the araldite and of the working electrode. For electrochemical impedance spectroscopy (EIS), a passive film was formed on the stainless steel, at -0.05 **V** for 1 **h,** in a 5% NaCl solution, at room temperature. A sinusoidal voltage perturbation of 10 **mV** and an applied frequency ranging from 100 **kHz** to 0.01 **Hz** were used. EIS was measured at the same voltage. Fitting was performed with the ZSimpwin software. The impedance spectra data were analysed with the simulation Boukamp equivalent circuit software[16].

3 Results

3.1 Microcosmic change

As shown in Fig. 1, the steel was available in the form of 2 **mm** thick cold rolled and annealed sheets, with an as received grain size of about 40-50 **μm**. Figure 2 (a) shows that when the α'-martensite nucleated at the intersection of two micro-shear bands, it resulted in the rolling process. From the nucleation characteristics, this type of martensite was referred to as strain-induced martensite, as proposed by Olson et al [7,17,18]. Stacking fault of as received 321 stainless steel, which was mainly due to the low stacking fault energy of the material (of approximately 30 $\mathbf{mJm^{-2}}$), can be seen in Fig. 2 (b). In addition, Fig. 3 (a) shows a few slip lines in the austenite grains. Figure 3 (b) shows the parallel and intersectional slipping lines that appeared in some grains. The number of the shear bands increased with increasing strain and stress. These microshear band intersections were stacking fault free-energy dependent as well as strain and strain rate-dependent[2]. The number of these intersections increased with decreasing SFE. As the number of these shear band intersections increased, it led to the nucleation of strain-induced martensite[19](Fig. 2). In addition, the density of slip bands varied from grain to grain, indicating a non-uniform deformation. Pitting corrosion was seen in the slip bands. Furthermore, microhardness measurements confirmed that the grains with dense slip bands were harder than those with sparse slip bands.

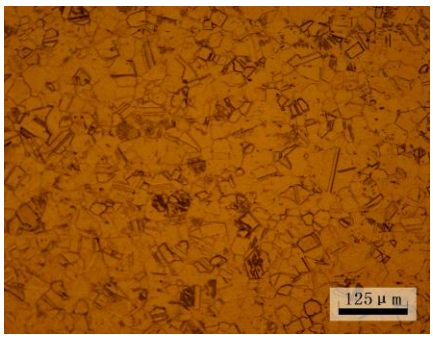

Fig. 1 Optical image of as received 321 stainless steel etching: 10% oxalic acid-etchant at room temperature.

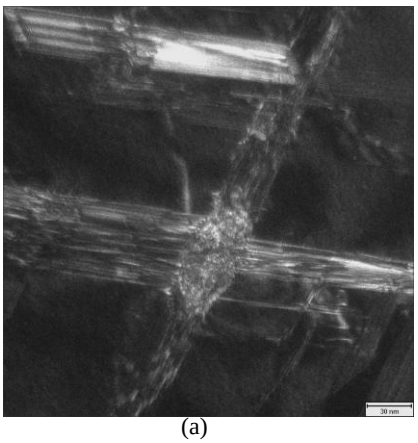

(a)

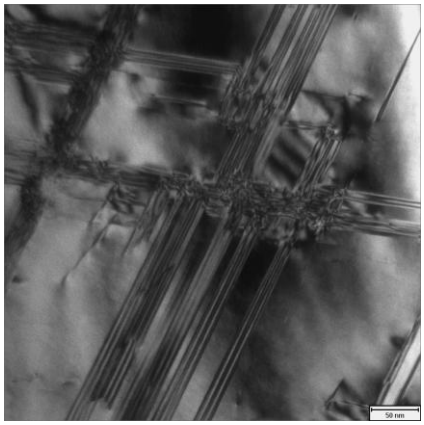

(b)

Fig. 2 (a) TEM image of α-martensite at intersection of two micro-shear bands and
(b) TEM image of stacking fault for as received 321 stainless steel.

(a)

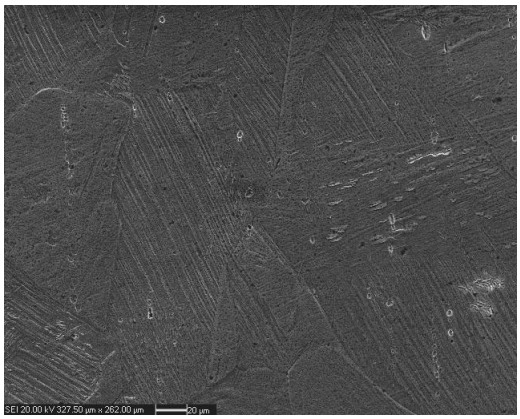

(b)

Fig. 3 SEM microstructure of AISI 321 stainless steel showing slipping lines of
(a) by 6% tensile deformation and
(b) by 25% tensile deformation.

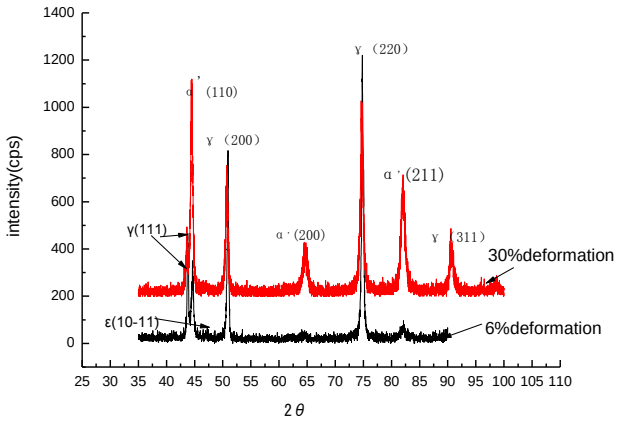

(a)

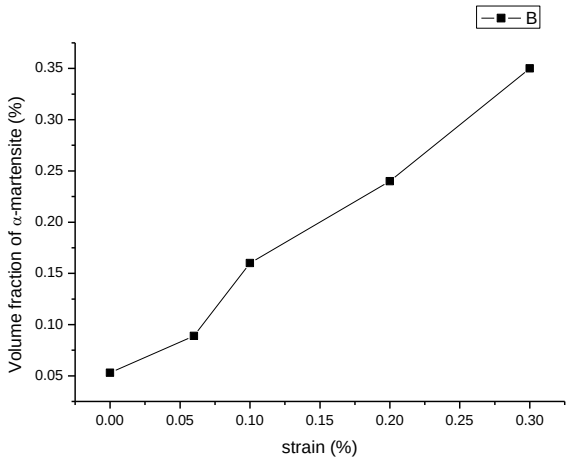

(b)

Fig. 4 (a) The XRD patterns for 6% and 30% tensile deformation of 321 ss at room temperature and
(b) Volume fraction of α'-martensite plotted as a function of engineering strain.

As shown in Fig. 4 (a), α-martensite reflections were detected in the strained samples by XRD. This indicated that strain-induced martensite was produced by tensile deformation at room temperature. Similar results are reported in the literature[7,20]. Multiple α-martensite transformation mechanisms viz: γ (fcc) $\rightarrow$ ε (hcp), γ (fcc) $\rightarrow$ α (bcc), γ (fcc) $\rightarrow$mechanical twins α (bcc) and γ (fcc) $\rightarrow\varepsilon$ (hcp) $\rightarrow$ α (bcc) have been observed during the deformation of AISI 304LN stainless steel at room temperature[20]. Quantitative analysis of the results is shown in Fig. 4 (b); ε-martensite with a $(10\bar{1}1)$ diffraction peak in the 6% deformation sample as in Fig. 4 (a), and its absence in the 30% deformation sample indicated that the deformation mode included $\gamma\rightarrow\varepsilon$-martensite $\rightarrow\alpha$-martensite and $\gamma\rightarrow\alpha$-martensite.

3.2 Electrochemical results

Figure 5 (a) and Table 2 illustrate that the deformation magnitude significantly affected the anodic polarization curve. The variation in the corrosion potential (E_{corr}), in the critical pitting potential(E_{pit}), and in the passive electric current(I_p) were not in line with the increasing cold work level. The most obvious, 10% deformation, showed the largest passivation current. A number of short-period current spikes were observed which were due to a metastable passivity breakdown followed by immediate repassivation (i.e., metastable pitting). The critical breakdown potential (E_{pit}) was defined as the voltage from where the current exhibits a sudden increase by a factor of over 100. As indicated by the arrow in Fig. 5 (a), a 20% deformation with a minimal critical pitting potential, could be seen, while the 6% and 30% deformed exhibited a higher break potential compared to other stainless steels in this experiment.

The higher the E_{pit} –value, the more resistant is the alloy to pitting corrosion, in the environment under consideration[21]. After improving the pitting resistance for a 6% tensile deformation, a decrease in the pitting resistance up to 10% (the largest passivation current) and 20% (the smallest break potential) tensile deformation and the increase in pitting resistance thereafter up to 30 tensile deformation were found. A similar result is reported in the literature [22]. The result will be explained hereafter, based on the microstructural changes observed in the specimens in section 4. After the experiments, the specimens were inspected visually, using low magnification SEM to verify the form of the possible corrosion. Triplicate tests were performed to verify the validity of the results. Tests where a crevice attack was observed were ignored. Several large pits with a diameter of roughly 40–60 **um** were found on the specimen surfaces after the potentiodynamic polarization tests, as shown in Fig. 5 (b), irrespective of the cold work level. Localized corrosion was mainly observed along the grain boundaries and along the deformation bands, in the 5% sodium chloride solution. From the above results, it is not difficult to see that the 10% and 20% deformed specimens could have the least corrosion resistance, while the 6% deformed specimen showed more resistance to corrosion in all experiments. In order to further validate this conclusion, electrochemical impedance spectroscopy (EIS) was carried out.

The polarisation curve is the most common accelerated electrochemical method used to study the pitting corrosion of austenitic stainless steels. For example in this type of test, several processes including dissolution, passivation, adsorption, diffusion, and others, are taking place. But it may be risky to use models based exclusively on direct current (dc) polarization data. Current–time transients at passive potentials are revealed in Fig. 6.

$$\frac{dL}{dt} = \frac{\bar{M}}{\bar{z} F \rho} i_p \tag{3}$$

$$I = 10^{-(A + k \lg t)} \tag{4}$$

The current decreased with time according to the formula (4)[23], and then it achieved a stable value.
where k represents the slope of the double-log plot for potentiostatic polarization. According to the literature[24], k =−1 indicated the formation of a compact, highly protective passive film, while k =−0.5 indicated the presence of a porous film, growing as a result of a dissolution and precipitation process. In this work, k equals between -0.19 and −0.55 for all specimens, which demonstrated the presence of a porous film. As a result, the bulk steel showed pitting.

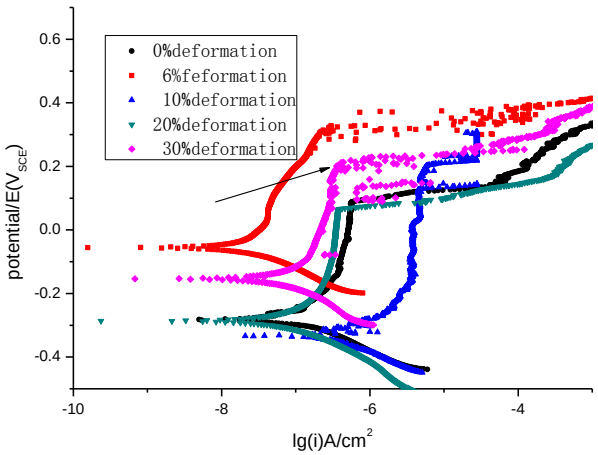

(a)

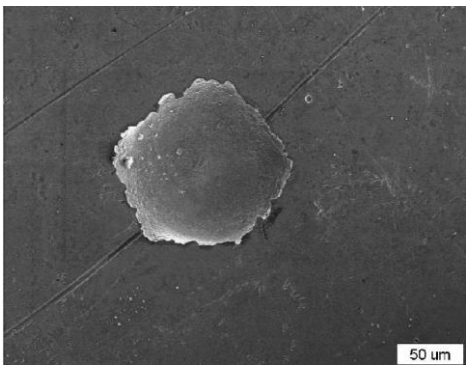

(b)

Fig. 5 (a) Potentiodynamic polarization curves for tensile deformation 321 ss in aerated 5% sodium chloride solution as a function of deformation level at room temperature, exhibiting a range of passivity beyond the open-circuit potential and
(b) SEM image of the pitted surface for the 10% deformation specimen after the potentiodynamic polarization.

Table 2 Variation in corrosion potential (E_{corr}), critical pitting potential (E_{pit}) and passive electric current lg(i) with engineer strain ε

ε	E_{corr}/V	E_{pit}/V	lg(i) A/cm^2
0%	-0.2831	0.094	-6.35
6%	-0.0565	0.3266	-7.07
10%	-0.3324	0.1935	-5.43
20%	-0.2824	0.081	-6.528
30%	-0.1545	0.21	-6.58

The analysis of impedance helped us to better understand the electrochemical behavior of the passive oxide layers formed on 321 stainless steels. The Nyquist plots (Fig. 7) showed unfinished semi-circle arcs. The equivalent circuit consisted of a constant phase element (interfacial capacitance) parallel to a polarization resistance (Rt), connected in series with an electrolyte resistance (R_{sol}). Fitting results were tabulated in Table 3. The formation of these semi-circle arcs was attributed to the charge transfer process in the electrode/electrolyte interface, relating to changes in the passive film property. The charge transfer resistance R_t was the smallest for the 20% deformation obtained, while it was maximal for the 6% deformation. This indicated that the 20% deformation presented the least corrosion resistance. The results of the EIS and of the polarization curve were consistent. In addition, R_{sol}, including the electrolyte resistance and other ohmic resistances, changed little in the NaCl solution. The constant phase element (CPE) represents a part of the non-faradaic electrode phenomena, namely the response of a developed non-ideal (dispersive) double layer capacitance. The factor n, defined as a CPE power, is an adjustable parameter that always lies between 0.5 and 1. When n=1, the CPE describes an ideal capacitor. For 0.5 < n < 1, the CPE describes a distribution of dielectric relaxation times in frequency space, and when n=0.5, the CPE represents a Warburg impedance of diffusional character. The CPE exponent *n*, having values between 0.8 and 0.89, reflects a dispersed capacitance. The same order of magnitude for values of Q can be seen in Y.X.QIAO *et. al*[25].

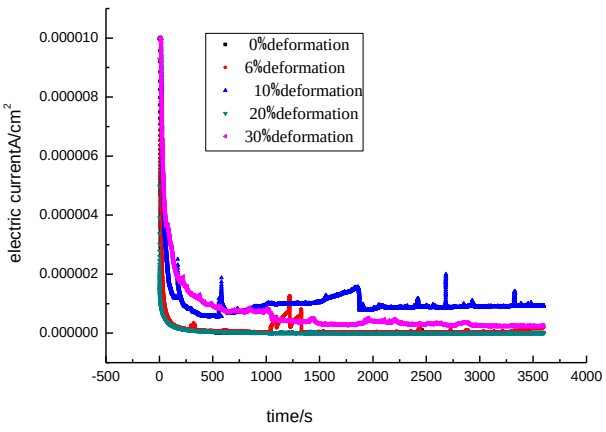

Fig. 6 Current–time transient responses at passive potentials generating in 5% NaCl solution and holding at -0.05 **V** for various tensile deformation specimens.

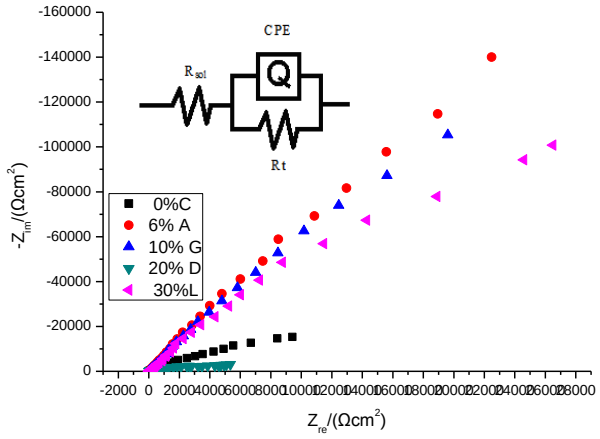

Fig. 7 Nyquist plot for the passive films of Type 321 ss in 5% NaCl solution with increasing deformation measured at applied potentials (-0.05**V**) for 1h and the equivalent circuit R(QR) used for quantitative evaluation of EIS spectra inserted in the upper corner.

Table 3 Equivalent circuit parameters for the tensile pre-deformation in 321 stainless steel

strain ε	R_{sol} (Ωcm^2)	Q ($\Omega^{-1}s^n cm^{-2}$)	n	Rt (Ωcm^2)
0%	12.99	5.14E-5	0.820	5.46E6
6%	15.37	9.08E-6	0.890	6.04E10
10%	24.25	1.33E-5	0.849	1.21E10
20%	18.04	5.57E-5	0.800	1.05 E5
30%	23.12	1.10E-5	0.880	2.28E6

4 Discussion

The effect of cold work on austenitic stainless steels was reported in earlier studies. The kinetics of strain-induced martensite formation in austenitic stainless steels were studied by Olson Cohen[7] and Hecker[6]. The transformation can be described by the Olson–Cohen analysis $f(\varepsilon)=1-\exp\{-\beta(1-\exp(-\alpha\varepsilon)^n\}$ [13] or $V_{\alpha'}=1-\exp(-\beta\varepsilon^n)$ [26] in uniaxial tension mode, where ε is the plastic strain, β is the stability parameter, and n is the deformation mode parameter. The volume fraction of α'-martensite phase in this analysis was approximately a sigmoidal function of strain under uniaxial tension loading. The α'-martensite that was introduced by tensile deformation in the ss deteriorated its corrosion resistance by selective anodic dissolution[10]. Besides, the properties of the stainless steel could be affected by a combination of various microstructural features, such as dislocation density, morphology, grain size and grain boundary substructure, to name only a few[27]. The pitting susceptibility varied with deformation. The variation in pitting potentials in a NaCl solution with increase in cold deformation is

also mentioned by several researchers[8,9,28].

A monotonous change in the pitting potential, exposed by some researchers, has been attributed to an increase in the volume fraction of α'-martensite[8,28]. In the present study the break potential, a nonlinear trend of pitting potential with increasing deformation, was found: the 20% deformed exhibited a minimal break potential, while the 30% deformed exhibited an elevated break potential. B. Ravikumar[29] also showed the highest recovery of pitting resistance after a drop in pitting potential at certain levels of cold work. In addition, the formation of passive film, which was considered useful to better understand the stress-corrosion-cracking behaviour of these materials on stainless steels, has been a subject of intense research for many years. A number of models were used to explain the kinetic, thermodynamic, structural and electronic properties of passive film for stainless steels. Point defect model (PDM)[30], which is based on the migration of the point defects (oxygen and metal vacancies) under the influence of the electrostatic field in the film, is widely accepted. In chloride-containing solutions, chloride ions can incorporate themselves in a passive film by occupying oxygen vacancies. The absorbed chloride ions would fill the anion vacancies (e.g. oxygen vacancies) and the system would respond to the loss of oxygen vacancies by generating cation vacancies: oxygen vacancy pairs via a Schottky-pair type of reaction (5)[30], where $V_M^{x'}$ and $V\ddot{o}$ represent, respectively, a cation vacancy and an oxygen vacancy. The newly generated oxygen vacancies could in turn react with additional chloride ions at the film-solution interface to generate more oxygen and cation vacancies. Therefore the absorption of chloride ions and the cation vacancy generation are autocatalytic. An increase in the generation rate of cation vacancies will promote the breakdown of a passive film. Research showed that the doping level of the oxide film formed on cold worked samples was higher than that of the passive film formed on annealed specimens[31].

$$Null \Leftrightarrow V_M^{x'} + \frac{\chi}{2} V_{\ddot{O}} \tag{5}$$

Increase in the passivation current by the low deformation (10% deformation in this work) could be the result of the formation of residual tensile stresses[32], which are known to be detrimental to corrosion resistance, and to the formation of deformation-induced α'-martensite[33,34], the latter indicating the effect of cold deformation parameters on the behaviour of the oxide film[35]. However, spontaneous passivation combined with enhanced surface chromium diffusion, resulting from the increased density of defects (Fig. 3), could contribute to the stable rich chromium passive film formation of up to 6% tensile deformation in a neutral chloride medium, thereby leading to improved pitting resistance[36]. In addition, the deformation-induced α'-martensite was very small for a 6% tensile deformation, which is also evidence of improved corrosion resistance. The high density of dislocation produced during plastic deformation introduced a defective passive film and the presence of strain-induced martensite in the structure, which led to the creation of a galvanic effect between the martensite and austenite phases[37,38]. These reasons may explain the reduced corrosion resistance of 20% deformation 321 stainless steel. There are two main reasons to the improved corrosion resistance properties for the 30% deformation. First, the passive film formed on highly deformed stainless steels contained a higher Cr/Fe ratio than that in the film on the non deformed one, and contributed to a higher pitting potential than for the latter[39,40]. This is because the diffusion rates of chromium along dislocations and in the martensite phase are higher than in the austenite phase[41]. Second, the large deformation texture in Fig. 4 (a) had a more important effect than the adverse effects of the residual stress and of the martensite.

5 Conclusion

The present study showed that the tensile deformation at room temperature had a complex influence on the corrosion resistance properties of 321 stainless steel. The main conclusions were that:

(1) Strain-induced martensite was produced for 321 austenitic stainless steel by tensile deformation at room temperature. Martensite transformation mechanisms included at least γ (fcc) $\rightarrow \alpha'$ (bcc) and γ (fcc) $\rightarrow \varepsilon$ (hcp) $\rightarrow \alpha'$ (bcc).

(2) A nonlinear trend of pitting potential with increasing deformation was found; after

improving the pitting resistance for 6% tensile deformation, 20% (the smallest break potential) tensile deformation seriously deteriorated the pitting corrosion resistance in chloride solutions. An increase in pitting resistance thereafter up to 30 tensile deformation was found. This result contradicts the hypothesis that strain-induced martensite is the main factor of corrosion resistance.

(3) The charge transfer resistance R_t was the smallest for the 20% deformation, and it was maximal for the 6% deformation. The results of the EIS and of the polarization curve were consistent.

(4) As the deformation changes to corrosion resistance were interpreted by selective anodic dissolution of strain-induced martensite, chromium diffusion, residual tensile stresses and deformation texture.

Acknowledgements

The authors gratefully acknowledge the facilities provided by the Material Tests Laboratory in the Science and Engineering School of Beijing University of Aeronautics and Astronautics. The assistance of Ms. Luo Hongyun and of Mr. Han Yuntao has also been greatly appreciated. This study was jointly supported by the Major Project of Chinese National Programs for Fundamental Research and Development (973 Program, 2006CB60500).

References

[1] WACHTER, O., and BRUMMER, G.: Experiences with Austenitic Steels in Boiling Water Reactors, Nuclear Engineering And Design, 1997, 168(1-3):35–52.

[2] HEUNG NAM HAN, CHANG GIL LEE, CHANG-SEOK OH, TAE-HO LEE, and SUNG-JOON KIM: A Model for Deformation Behavior and Mechanically Induced Martensitic Transformation of Metastable Austenitic Steel, Acta Materialia, 2004, 52 (17):5203–5214.

[3] PEGUET, L., MALKI, B., and BAROUX, B.: Influence of Cold Working on the Pitting Corrosion Resistance of Stainless Steels, Corrosion Science, 2007, 49 (4):1933–1948

[4] YAO FU, XINQIANG WU, EN-HOU HAN, WEI KE, KE YANG, and ZHOUHUA JIANG: Effects of Cold Work and Sensitization Treatment on the Corrosion Resistance of High Nitrogen Stainless Steel in Chloride Solutions, Electrochimica Acta, 2009, 54 (5):1618–1629

[5] VERCAMMEN, S., BLANPAIN, B., DE COOMAN, B. C., and WOLLANTS, P.: Cold Rolling Behavior of an Austenitic Fe–30Mn–3Al–3Si TWIP-Steel: the Importance of Deformation Twinning, Acta Materialia, 2004, 52 (7): 2005–2012

[6] HECKER, S.S., STOUT, M.G., STAUDHAMMER, K.P., and SMITH. J.L.: Effect of Strain State and Strain Rate on Deformation Induced Transformation in 304 Stainless Steel Magnetic Measurements and Mechanical Behavior, Metall Trans, 1982, 13(A):619– 626.

[7] OLSON, G.B., and MORRIS, C.: A Mechanism for the Strain-Induced Nucleation of Martensitic Transformations, Journal of the Less Common Metals, 1972, 28(1):107-118

[8] MAZZA, B., PEDEFERRI, P., SINIGAGLIA, D., CIGADA, A., MONDORA, G.A., RE, G., TACCANI, G., and WENGER, D.: Pitting Resistance of Cold-Worked Commercial Austenitic Stainless Steels in Solution Simulating Seawater, Journal of the Electrochemical Society, 1979, 126(3):2075.

[9] SEMINO, C.J., PEDEFERRI, P., BURSTEIN, G.T., and HOAR, T.P.: The Localized Corrosion of Resistant Alloys in Chloride Solutions, Corrosion Science, 1979, 19(12):1069-1078.

[10] RAVI KUMAR, B., RAGHUVIR SINGH, BHUPESHWAR MAHATO, DE, P.K., and BANDYOPADHYAY, N.R.: Bhattacharya, D.K., Effect of Texture on Corrosion Behavior of AISI 304l Stainless Steel, Materials Characterization, 2005, 54(2):141– 147.

[11] SCHWIND, M., KÄLLQVIST, J., NILSSON, J.O., ÅGREN, J., and ANDRÉN, H.O.: σ -PHASE Precipitation in Stabilized Austenitic Stainless Steels, Acta Materialia, 2000, 48(10):2473-2481.

[12] PARDO, A., MERINO, M.C., COY, A.E., VIEJO, F., CARBONERAS, M., and ARRABAL, R.: Influence of Ti, C and N Concentration on the Intergranular Corrosion Behavior of AISI 316Ti And 321 Stainless Steels, Acta Materialia, 2007, 55(7):2239–2251.

[13] ANGEL, T.J.: Formation of Martensite in Austenitic Stainless Steels. Journal of the Iron and Steel Institute, 1954, 177:165–174.

[14] ASTM, Designation, 1994, A 262-293, 1.

[15] MORDYUK, B.N., PROKOPENKO, G.I., VASYLYEV, M.A., and IEFIMOV, M.O.: Effect of Structure Evolution Induced by Ultrasonic Peening on the Corrosion Behavior of AISI-321 Stainless Steel, Materials Science and Engineering A, 2007, 458(1-2):253–261.

[16] BERNARD, A., and BOUKAMP: A Nonlinear Least Squares Fit Procedure for Analysis of Immittance Data of Electrochemical Systems, Solid State Ionics, 1986, 20(1):31-44.

[17] WOEI-SHYAN LEE, and CHI-FENG LIN: The Morphologies and Characteristics of Impact-Induced Martensite in 304 Stainless Steel, Scripta Mater, 2000, 43(8):777–782.

[18] STAUDHAMMER, K.P., MURR, L.E., and HECKER, S. S.: Nucleation and Evolution of Strain-Induced Martensite Embryos and Substructure in Stainless Steel: A Transmission Electron Microscopy Study, Acta Metallurgica, 1983, 31(2):267-274.

[19] ARPAN DAS, and SOUMITRA TARAFDER: Experimental Investigation on Martensitic Transformation and Fracture Morphologies of Austenitic Stainless Steel, International Journal of Plasticity, 2009, 25(11):2222–2247.

[20] ARPAN DAS, SIVAPRASAD, S., GHOSH, M., CHAKRABORTI, P.C., and TARAFDER, S.: Morphologies and Characteristics of Deformation Induced Martensite during Tensile Deformation of 304 LN Stainless Steel, Materials Science and Engineering A, 2008, 486(1-2):283–286.

[21] JONES, DA.: Principles and prevention of corrosion. New York: Macmillan Publishing Company, 1992.

[22] RAVI KUMAR, B., RAGHUVIR SINGH, MAHATO BHUPESHWAR, DE, P.K., BANDYOPADHYAY, N.R., and BHATTACHARYA, D.K.: Effect of Texture on Corrosion Behavior of AISI 304l Stainless Steel, Materials Characterization, 2005, 54(2):141– 147.

[23] IGOR NICIC, MACDONALD, and DIGBY, D.: The Passivity of Type 316l Stainless Steel in Borate Buffer Solution, Journal of Nuclear Materials, 2008, 379(1-3):54–58.

[24] LAKATOS-VARSANYI, M., FALKENBERG, F., and OLEFJORD, I.: The Influence of Phosphate on Repassivation of 304 Stainless Steel in Neutral Chloride Solution, Electrochimca Acta, 1998, 43(1-2): 187-197.

[25] QIAO Y.X., ZHENG Y.G., KE W., and OKAFOR P.C.: Electrochemical Behavior of High Nitrogen Stainless Steel in Acidic Solutions, Corrosion Science, 2009, 51: 979–986.

[26] HAUŠILD, P., DAVYDOV, V., DRAHOKOUPIL, J., LANDA, M., and PILVIN, P.: Characterization of Strain-Induced Martensitic Transformation in a Metastable Austenitic Stainless Steel, 2010, Materials and Design, 31(4):1821–1827.

[27] MARSHAL, P.: Austenitic Stainless Steel: Microstructure and Mechanical Properties, London, Elsevier Science, 1985: 294

[28] ECKSTEIN, C., WELSS, A., JANKE, D., and PEISKER, D.: Stainless Steels 99, Italy, June 6–9, Science and Market, 1999.

[29] RAVIKUMAR, B., MAHATO, B., and RAGHUVIR SINGH: Influence of Cold-Worked Structure on Electrochemical Properties of Austenitic Stainless Steels, Metallurgical and Materials Transactions A, 2007, 38(A):2085-2093.

[30] CHAO, Y., LIN, L.F., and MACDONALD, D.D.: A Point Defect Model for Anodic Passive Films, J. Electrochem. Soc. 1981, 128:1187.

[31] RANGEL, C.M., and SILVA, T.M.: Semiconductor Electrochemistry Approach to Passivity and Stress Corrosion Cracking Susceptibility of Stainless Steels, Electrochimica Acta, 2005, 50(25-26):5076–5082.

[32] HANNINEN, HE.: Influence of Metallurgical Variables on Environment-Sensitive Cracking of Austenitic Alloys, International Materials Reviews, 1979, 3:85–135.

[33] TORKAR, M.: Corrosion of AISI 316 Ti in 50% Koh due to Deformation Induced Martensite, Engineering Failure Analysis, 2006, 13(4):624–628.

[34] PEGUET, L., and MALKI, B.: Effect of Austenite Stability on the Pitting Corrosion Resistance of Cold Worked Stainless Steels, Corrosion Science, 2009, 51(3):493–498.

[35] BARBUCCHI, A., DELUCCHI, M., PANIZZA, M., SACCOM, and CERISOLA, G.: Electrochemical and Corrosion Behavior of Cold Rolled AISI 301 in 1 MH_2SO_4, Journal of Alloys and Compounds, 2001, 317-318, 607–611.

[36] KAMACHI MUDALI, U., and SHANKAR, P.: On the Pitting Corrosion Resistance of Nitrogen Alloyed Cold Worked Austenitic Stainless Steels, Corrosion Science, 2002, 44(10) :2183–2198.

[37] SEETHARAMAN, V., and KRISHNAN, R.: Influence of the Martensitic Transformation on the Deformation Behavior of an AISI 316 Stainless Steel at Low Temperatures, Journal of Materials Science, 1981, 16(2): 523–530.

[38] HAMADA, A.S., KARJALAINEN, L.P., and SOMANI, M.C.: Electrochemical Corrosion Behavior of a Novel Submicron-Grained Austenitic Stainless Steel in an Acidic NaCl Solution, Materials Science and Engineering: A, 2006, 431(1-2): 211–217.

[39] BARBUCCI, A., CERISOLA, G., and CARBOT, PL.: Effect of Cold Working in the Passive Behavior of 304 Stainless Steels in Sulfate Media, Journal of the Electrochemical Society, 2002, 149(B): 534-542.

[40] PHADNIS, SV., SATPATI, AK., MUTHE, KP., VYAS, JC., and SUNDARESHAN, JC.: Comparison of Rolled and Heat Treated SS304 In Chloride Solution Using Electrochemical and XPS Techniques, Corrosion Science, 2003, 45(11):2467–2483.

[41] KAIN, V., and CHANDRA, K.: Effect of Cold Work on Low-Temperature Sensitization Behavior of Austenitic Stainless Steels, 2004, Journal of Nuclear Materials, 334(2-3):115–132.